Generalized Fourier Holography Meets Coherent Diffractive Imaging

A. J. D'Alfonso,[1]* A. V. Martin,[2] A. J. Morgan,[1] P. Wang,[3] H. Sawada,[4] A. I. Kirkland,[5] and L. J. Allen[1]

[1]School of Physics, University of Melbourne, Parkville, Victoria 3010, Australia

[2]ARC Centre of Excellence for Coherent X-ray Science, School of Physics, University of Melbourne, Parkville, Victoria 3010, Australia

[3]National Laboratory of Solid State Microstructures and Department of Materials Science and Engineering, Nanjing University, Nanjing 210093, People's Republic of China

[4]JEOL Ltd, 1-2 Musashino 3-Chome, Akishima, Tokyo 196, Japan

[5]Department of Materials, University of Oxford, Parks Road, Oxford OX1 3PH, UK

*ad@unimelb.edu.au

Introduction

Imaging a specimen of condensed matter, broadly speaking, has been limited by the precision to which imaging lenses can be manufactured and their aberrations controlled. The exit-surface wave, which is the probing radiation after transit and interaction with the specimen, contains a representation of a specimen's structure. This has prompted significant research efforts into methods that are able to reconstruct the exit-surface wave without the use of imaging optics (without lenses). Coherent diffractive imaging (CDI) is an imaging technique that seeks to restore the exit-surface wave from intensity measurements, either in the far-field diffraction plane or the near-field Fresnel diffraction region. Coherent diffractive imaging allows unaberrated representations of the specimen, in terms of both the amplitude and phase of the exit-surface wave, to be obtained that are limited only by the wavelength of the incident radiation. To date, numerous strategies have been proposed to complete this restoration, the most successful being the original scheme proposed by Gerchberg and Saxton [1] and its subsequent modifications. These schemes all involve the iterative refinement of a trial wave function using *a priori* known information about the sample in conjunction with the wave amplitude (the square root of the measured intensity) to constrain the proposed phase of the exit-surface wave. These approaches use the self-interference of the exit-surface wave to transform the reconstruction process into a non-smooth, non-convex, non-linear optimization problem and as such are plagued by uniqueness issues. A typical experimental setup of a coherent diffractive imaging experiment is shown in Figure 1.

Concurrent to developments in CDI have been extensions to Fourier holography [2]. In traditional Fourier holography the measured interference, in the far-field diffraction plane, between a reference wave generated by a "pinhole source" and the unknown scattered wave is used to deduce the complex exit-surface wave. Under these special conditions the image reconstruction procedure from the diffracted intensity measurement is direct—a single inverse Fourier transform of the diffraction data producing a unique solution. The maximum frequency to which this interference can be reliably recorded, limits the resolution of the reconstruction procedure. For a perfect pinhole this limit is the wavelength of the probing radiation. The Fourier holography inversion procedure is analytic, and consequently deviations away from a perfect pinhole reference introduces errors into the reconstruction. This is particularly pertinent because by reducing the size of the pinhole, in order to improve the reconstruction resolution, a concurrent decrease in the reference wave intensity occurs and the resolution of the reconstruction procedure becomes flux-limited. The unfavorable coupling of flux and resolution has motivated extensions to Fourier holography, allowing corners, ultra-redundant arrays, and Fresnel zone plates to be used as the source of the reference wave.

Recently results obtained using a generalized approach to Fourier holography [3, 4] have been reported. This generalized holography method allows the use of an arbitrary reference wave and has been applied at the micrometer, nanometer, and atomic scale using visible light, X-ray radiation, and electron probes, respectively. This article summarizes some results from this approach.

Materials and Methods

Algorithm description. Using a generalized approach to Fourier holography [3, 4] allows the autocorrelation of the exit-surface wave, which is the inverse Fourier transform of the diffraction pattern, to be analyzed and a set of linear equations to be constructed. Solving this set of linear equations allows the direct reconstruction of the exit-surface wave. Key to the algorithm is the analysis of the autocorrelation plane. Expressing the exit wave as the sum of the reference wave and the scattered wave, the autocorrelation is processed by subtracting the autocorrelation of the known reference wave and subsequently identifying regions remaining in the autocorrelation data

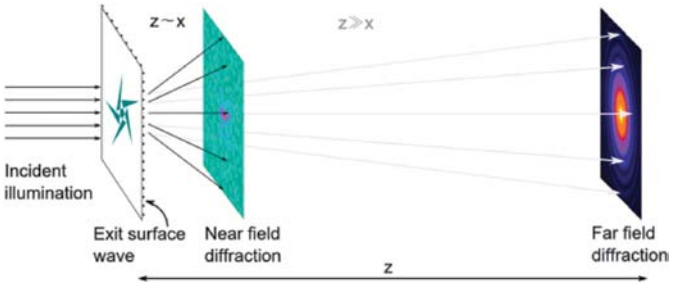

Figure 1: Schematic of the coherent diffractive imaging geometry. Incident illumination scatters from the object, of a characteristic length scale x, producing an exit surface wave. The complex exit surface wave then propagates in space, indicated by the distance z, where the intensity is recorded in the near field or the far field.

it's here!

EMS is happy to announce our new

Full Line Catalog XVII

loaded with hundreds of new products...
loaded with helpful technical tips...
loaded with techniques and applications...

The most comprehensive source for all fields of microscopy and general laboratory research

It is with great pleasure we continue to offer to you our outstanding selection of Chemicals for Electron Microscopy, Light Microscopy and Histology; the industry-leading line of Aurion ImmunoGold Reagents; the highest quality, most precise sectioning and incomparable durability DiATOME Diamond Knives line, our superb line of EMS Sputter and Carbon Coaters, world-renowned Technovit® embedding resins, and the list goes on. Most of these lines have been enhanced with new options. We hope that this catalog exceeds your expectations and we look forward to working with you.

NEW: EVOS Digital Microscopes

CryoJane Workstation

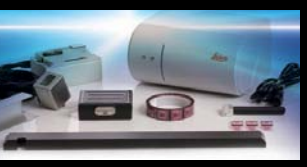

NEW: Rotary Diamond Micro-Engraver Pen

NEW MODELS: Vibrating Microtomes

NEW: Turbo-Pumped Sputter/ Carbon Coater for Glove Box

NEW: HistoPro® 200

NEW: Athene Grids

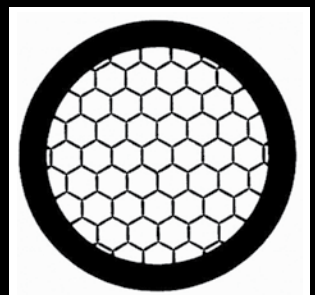

NEW: FLOWMI™ Cell Strainers

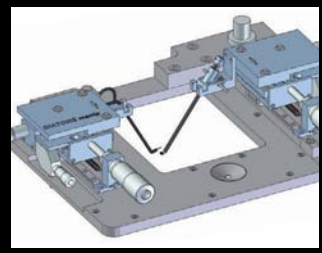

NEW: DiATOME manipulator

NEW: INFINITY 3-3UR Research-Grade Microscopy Camera

NEW: EMS High-End Medical Tweezers

NEW MODELS: Branson Ultrasonic Benchtop Cleaners

REQUEST YOUR COPY AT
www.emsdiasum.com

Electron Microscopy Sciences

P.O. Box 550 • 1560 Industry Rd. • Hatfield, Pa 19440
Tel: (215) 412-8400 • Fax: (215) 412-8450
email: sgkcck@aol.com *or* stacie@ems-secure.com

look for us...

YouTube

that are either linear or non-linear in the scattered wave. Provided the reference wave satisfies the conditions as outlined in reference [3], there will be a sufficient quantity of linear information so that the exit wave may be determined by solving the non-singular matrix equation. Furthermore, as the coefficient matrix has a Hankel-plus-Toeplitz-like structure, the solution to the matrix equation may be solved efficiently using the conjugate gradients least squares method, implemented using fast Fourier transforms. Full details of the reconstruction algorithm and its mathematical underpinnings are discussed in reference [4], and a free version is available for download [5].

Results

Visible light. The first proof-of-principle demonstration of the procedure was applied using visible light. The diffraction pattern formed by an Australian gnat's wing using a HeNe laser (wavelength 632.8 nm) is shown in Figure 2a. The incident beam was attenuated using a neutral density filter before spatial filtering by focusing through a 20 µm pinhole. It was then re-collimated by a lens of focal length 250 mm to obtain an approximately planar monochromatic beam. This beam then illuminated a conical hole formed in a 3 mm thick stainless-steel disk with the sides of the hole tapered by 15° and with the larger diameter facing the beam. The object was fixed with adhesive to the outside of the smaller-diameter aperture, which had a diameter of 2.035 ± 0.005 mm. The tapering of the hole avoided diffraction effects associated with the first aperture. This geometry results in an assumed aperture/illumination in the object plane as shown in Figure 2b, and a high-resolution microscope image of the object in the region that the object was confined to, with respect to the aperture, is shown in Figure 2c. Figures 2a and 2b show the total data input, plus the object area (shown in the lower part of the illumination in Figure 2c) that is required for the reconstruction.

To record the diffraction pattern, an antireflection coated, planoconvex lens of focal length 75 mm was located 1 mm downstream of the object and focused onto the surface of a monochrome CCD camera (a Prosilica GE1650). This CCD has 1600 × 1200 pixels that are each 7.4 µm squared with a 12-bit per pixel dynamic range, ensuring that the interference between the sample and the reference wave was sampled to high resolution in the detector plane.

Using the generalized holography reconstruction algorithm with inputs shown in Figures 2a–2c, (excluding the wing), the exit wave amplitude and phase were reconstructed and are presented in Figures 2d and 2e, respectively. The exit wave reconstruction results shown in Figures 2d and 2e used 550 iterations of the generalized holography reconstruction algorithm [4] and needed on the order of minutes to compute on a standard desktop computer. Immediately of note is the good representation of the amplitude and phase of the gnat's wing, the former comparing favorably with a light microscope image in Figure 2c. The good-quality reconstructions coupled with the rapid reconstruction procedure allows us to envisage that with purpose-written multiprocessor code one could perform real-time reconstructions.

X-ray radiation. The visible light example in the preceding section used the general case of the known scattering from a confined region of a circular aperture as the reference wave. A demonstration of the broad flexibility of the reconstruction algorithm and its application using truly arbitrary illuminations was demonstrated recently [6] using free electron laser pulsed X-ray illumination. The experiment was performed at FERMI [7], a seeded soft X-ray free-electron laser. The pulses produced by FERMI had a wavelength of 32.5 nm and are estimated to be 100 fs in duration. The focal spot of the beam was ~15 × 30 µm^2. After the gas attenuator the pulse energy was 10–15 mJ. The beam was attenuated a further 1.25% by aluminium filters. The X-ray pulses were incident onto a platinum nanoscale structure deposited onto a Si_3N_4 window, and it is shown in Figure 3a. The diffraction pattern measurement was constructed by integrating 100 pulses,

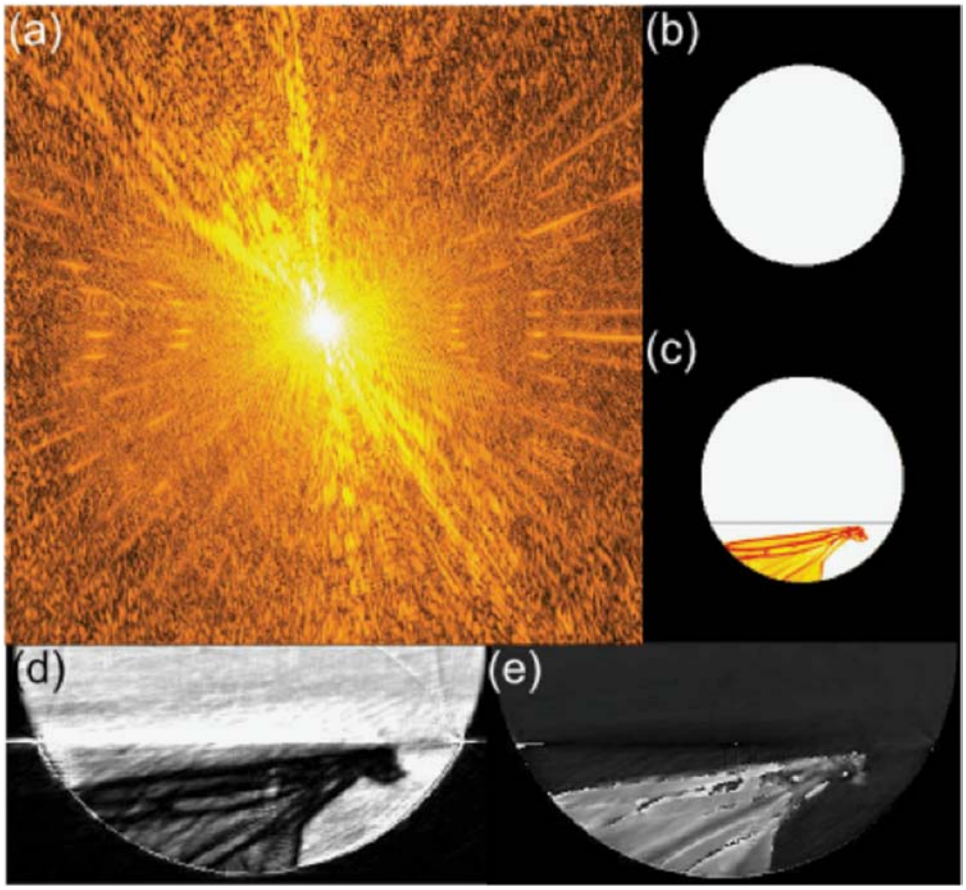

Figure 2: (a) Diffraction pattern formed by illumination of a gnat's wing with a HeNe laser. (b) Assumed illumination intensity and phase. (c) Light microscope image of the object in the area within which the object is contained relative to the illumination. Reconstructed exit wave amplitude (d) and phase (e). Diffraction data, reconstruction results, and figures are taken from reference [4], reprinted with permission of the American Physical Society, copyright 2012.

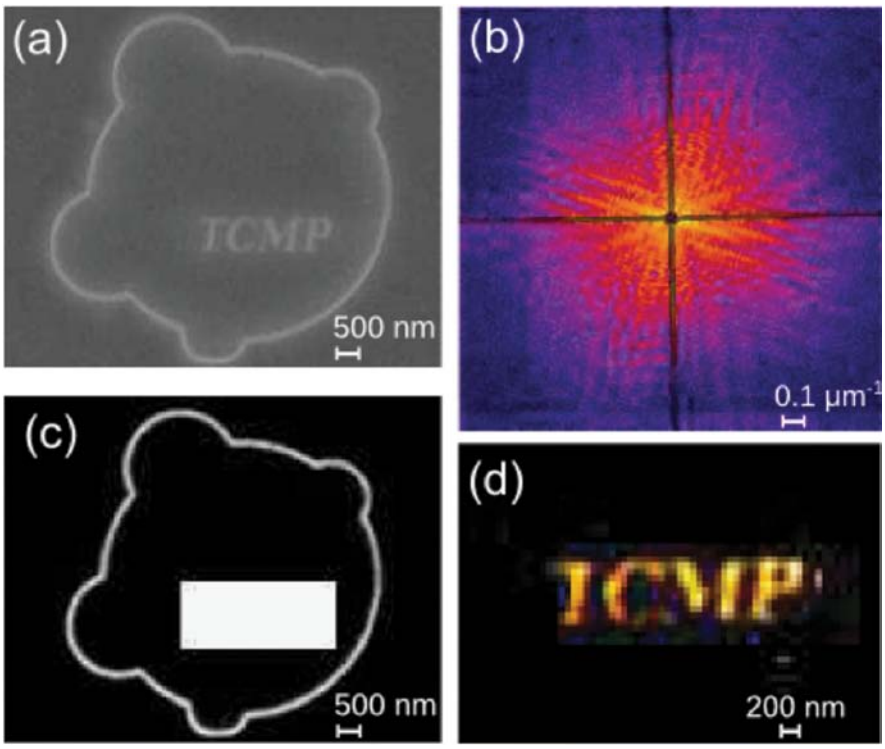

Figure 3: (a) SEM image of the sample. (b) Diffraction pattern showing regions of missing data. (c) Constructed reference wave and object area. (d) Reconstructed exit wave intensity. Diffraction data, reconstruction results, and figures are taken from reference [6], reprinted with permission of the Nature Publishing Group, Macmillan Publishers Limited, copyright 2014.

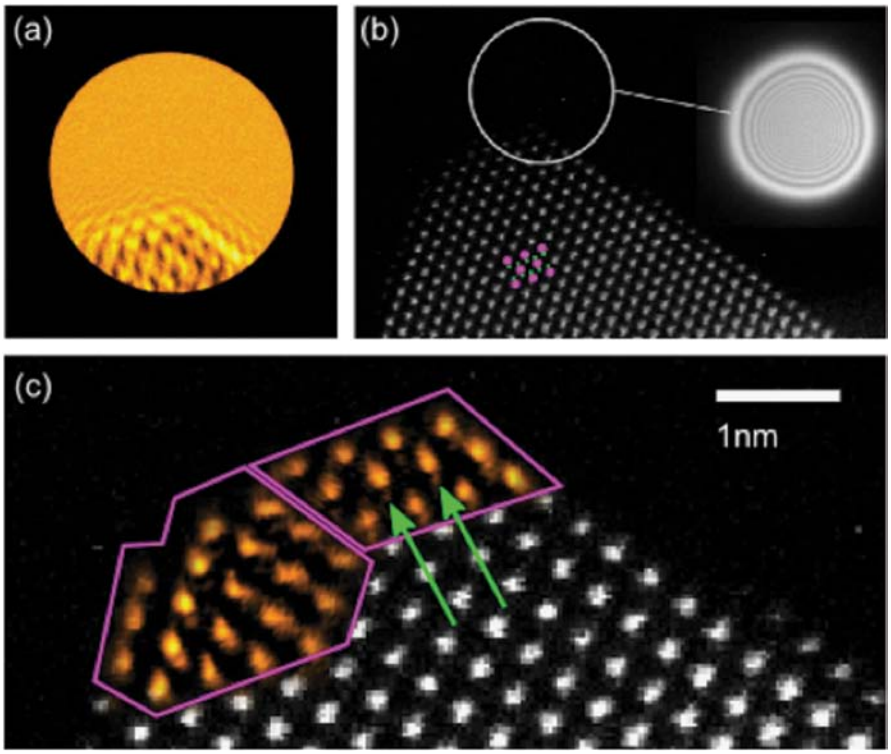

Figure 4: (a) Diffraction pattern (shadow image) of a CeO_2 nanoparticle obtained using a defocused STEM probe. (b) HAADF image with the computed probe amplitude. The position of the probe for the diffraction pattern in (a) is indicated by the circle over the top right corner in (b). The projected structure of CeO_2 is indicated. The larger pink circles indicate cerium columns, and the smaller green circles indicate oxygen columns. (c) Two independent reconstructions, indicated by the magenta outlines, of the phase of the transmission function are overlaid onto the HAADF image of the specimen. The green arrows indicate the position of the O columns adjacent to the Ce columns. Diffraction data, reconstruction results, and figures are taken from reference [8], reprinted with permission of the American Physical Society, copyright 2013.

and is shown in Figure 3b. The diffraction pattern was acquired using a 32.5-nm multilayer mirror that reflects the scattered photons on a CCD detector (Princeton instrument MTE2048B, 13.5 μm pixel size) with the maximum scattering angle being about 14 degrees, the black shaded regions in Figure 3(b) refer to a missing data region of 0.4 degrees, necessary to prevent CCD damage. The maximum spatial frequency recorded by the detector was $2\pi \times 0.017\,nm^{-1}$. From the scanning electron microscopy (SEM) image in Figure 3a, the reference wave was defined and the central rectangular region containing the letters "TCMP" was the unknown object area. The reference wave with respect to the object area is shown in Figure 3c. From the given inputs depicted in Figures 3b and 3c, the exit-surface wave intensity was reconstructed to a half-period resolution of approximately 170 nm and is shown in Figure 3d. The excellent reconstruction obtained using the arbitrary reference wave has clear ramifications for future experiments and imaging modes.

Electron microscopy. The generalized holography reconstruction procedure also has been successfully applied at atomic resolution using conventional scanning transmission electron microscopy (STEM) [8]. Significantly, no special modifications or esoteric optical arrangements were required to perform the experiment suitable for the reconstruction procedure. To perform the experiment, a JEOL R005 aberration-corrected STEM with a cold field-emission gun (FEG) operating at an accelerating voltage of 300 kV and with a probe-forming convergence semi-angle of 24 mrad was used (implying an intrinsic resolution of 0.08 nm in real space). The coherent electron probe was defocused onto the sample plane so that it was able to form a shadow image of the specimen in the diffraction plane. This is also known as a Gabor hologram or Ronchigram. The recorded diffraction pattern used for the reconstruction, obtained from a cerium dioxide nanoparticle, is shown in Figure 4a. The diffraction pattern was recorded using a Gatan Ultrascan 1000 CCD camera with a nominal camera length of 12 cm and a pixel size in the detector plane of 14 μm.

In this particular experiment the reference wave was the un-scattered portion of the electron probe. Characterization of the phase-related properties of the illuminating probe was obtained from the aberrations of the electron optical-system measured using the microscope aberration-corrector software. A probe defocus of 77 nm and the

measured aberrations implied an incident probe intensity at the specimen as shown in the top right corner of Figure 4b. The circle overlapping the edge of the nanoparticle indicates the position of the probe over the nanoparticle for the diffraction measurement. Using the diffraction pattern in Figure 4a and the complex illumination in Figure 4b, the specimen transmission function was reconstructed leading to the phase image of the reconstructed sample transmission function shown in Figure 4c overlaid on top of a STEM Z-contrast image of the sample. Immediately clear is the good one-to-one correspondence between the reconstruction and the Z-contrast image. More interestingly, since the contrast of a STEM Z-contrast image scales with atomic number as approximately $Z^{1.7}$, the relative differences between the atomic number of cerium and oxygen implies that both atom types are not visible simultaneously in the Z-contrast image. This is not the case for the phase image, and the oxygen columns, indicated by green arrows, can be seen on either side of the cerium columns in positions that correspond to the known cerium dioxide structure, schematically indicated in Figure 4c.

Conclusion

Fourier holography is a lensless imaging technique that is direct and promises to circumvent some of the limitations associated with more conventional imaging techniques, for example, imperfect lenses. Furthermore, unlike traditional coherent diffractive imaging, which employs a non-linear image reconstruction procedure, Fourier holography solves a set of linear equations and is not plagued by non-unique solutions. However, to date Fourier holography has been hampered by the unfavorable coupling of reference flux and resolution.

This article presents the application of a generalized holographic exit wave reconstruction procedure using a broad spectrum of different illumination types. The technique retains the favorable aspects of Fourier holography while decoupling resolution and reference flux. The generalized holographic approach used here allows a wide range of reference waves to be tailored to specific imaging conditions, for instance optimizing radiation dose and resolution, to allow single-shot imaging applications. Perhaps the most significant advantage presented is that the burden on fabricating perfect references for use in Fourier holography is shifted toward the characterization of reference scatterers. This subtle change of perspective serves to improve the robustness of the reconstruction procedure and relax constraints on experimental design.

References

[1] RW Gerchberg and WO Saxton, *Optik* 35 (1972) 237–46.
[2] S Eisebitt et al., *Nature* 432 (2004) 885–88.
[3] AV Martin and LJ Allen, *Opt Comm* 281 (2008) 5114–21.
[4] AJ D'Alfonso et al., *Phys Rev A* 85 (2012) 013816–24.
[5] http://tcmp.ph.unimelb.edu.au/mustem
[6] AV Martin et al., *Nat Commun* 5 (2014) doi:10.1038/ncomms5661.
[7] E Allaria et al., *New J Phys* 12 (2010) doi:10.1088/1367-2630/12/7/075002.
[8] AJ Morgan et al., *Phys Rev B* 87 (2013) 094115–20.

MT

REACH FOR THE HIGHEST RESOLUTION AT THE ATOMIC SCALE

ARM300F

THE GRAND ARM

Proven performance — unmatched raw data.
The highest resolution commercially-available Atomic Resolution TEM in the world.

- 63 picometer point-to-point resolution guaranteed
- 80-300 kV cold FEG
- Large solid angle SDD for atomic level chemistry
- Available with or without Cs correctors for TEM and STEM
- All-JEOL column optics and software
- Ultimate stability
- Renowned service and support

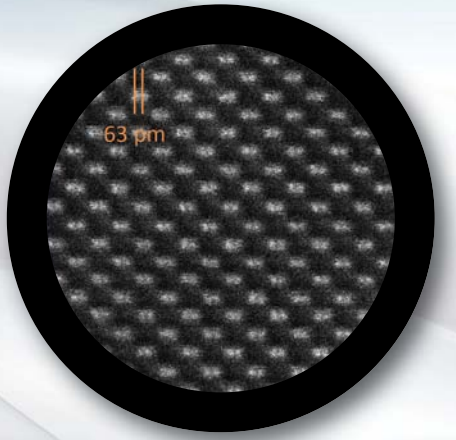

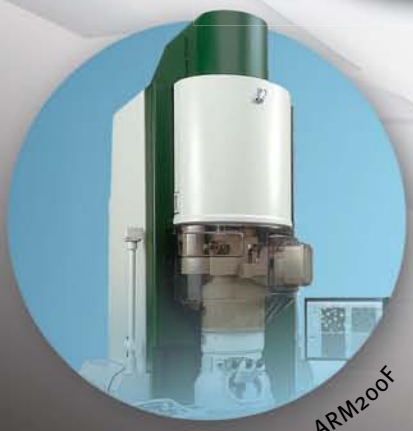
ARM200F


ARM200F/CFEG

JEOL
Solutions for Innovation

www.jeolusa.com
salesinfo@jeol.com • 978-535-5900

REALab

https://doi.org/10.1017/S1551929514001382 Published online by Cambridge University Press